Global NEST Journal, Vol 25, No 9, pp 150-158

Bio-inspired synthesis of CuO and ZnO nanoparticles by hydrothermal method: characterization and evaluation as photocatalytic degradation of imidacloprid pesticide

Amna Iqbal[1,*], Atta ul Haq[1], Lesli Rios-Aspajo[2] and Andres Iturriaga-Chavez[3]

[1]Department of Chemistry, Government College University Faisalabad, 38000, Pakistan

[2]Centro de investigación y Desarrollo Tecnológico Industrial (CIDTI), Analyzen Peru S.A.C., Mz. S. Lt. 1 asociación Villa la Paz de Jicamarca, Huarochirí, Anexo 22, Lima, Perú

[3]Departamento de investigación y desarrollo tecnológico de aguas residuales (DIDAR), Limaem S.A.C., Morro Solar 230, dpto. 1002, Santiago de Surco, Lima, Perú

Received: 06/08/2023, Accepted: 20/09/2023, Available online: 02/10/2023

*to whom all correspondence should be addressed: e-mail: 2016-gcuf-000028@gcuf.edu.pk

https://doi.org/10.30955/gnj.005285

Graphical abstract

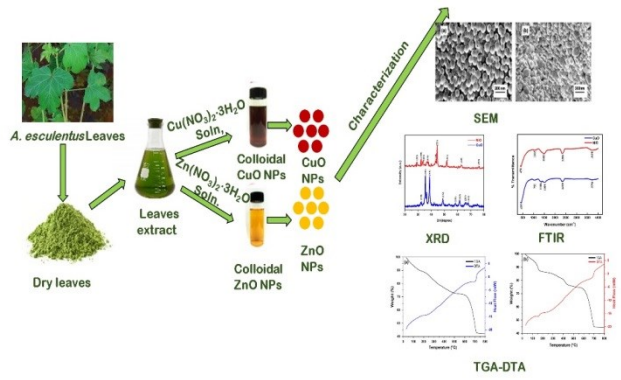

Abstract

In this work, copper oxides (CuO) and zinc oxide (ZnO) nanoparticles were synthesized using *Abelmoschus esculentus* (*A. esculentus*) leaves extract by hydrothermal method and subsequently employed for degrading recalcitrant pesticide imidacloprid (IMI). The CuO and ZnO nanoparticles were characterized by UV–Vis, FTIR, XRD, HR-SEM and TGA/DTA. The band gap of CuO and ZnO nanoparticles has been calculated to be about 2.23 eV and 3.6 eV respectively. The average size of CuO and ZnO nanoparticles calculated were in the range of 24–33 nm and 18–35 nm respectively which was confirmed by HR-SEM and XRD. The XRD studies indicated that the synthesized nanoparticles have a face-centered cubic structure. Photocatalytic degradation study showed nanoparticles bear a good potential to degrade IMI. The degradation was found to be affected by the IMI concentration (10–70 mg L^{-1}), solution pH (5–11) and photocatalyst dosages (0.1-0.5 g L^{-1}). The optimum experimental conditions (i.e., Photocatalyst dosage = 0.5g, pH = 9, IMI conc. 30 mgL^{-1} and contact time = 50 min) for the photocatalytic degradation process using CuO and ZnO led to IMI removal of 99% and 81% respectively in 60 min. The pesticide degradation percentage in the case of CuO photocatalyst were outstanding and reached ~99%, while for ZnO photocatalyst it was ~81%. The Kinetic study showed that the degradation of IMI was well foreseen by pseudo-first order kinetic model. For CuO and ZnO photocatalysts the rate constants were 0.028/min and 0.0076/min respectively. The prepared photocatalysts showed excellent water stability and reusability.

Keywords: Green synthesis, *Abelmoschus esculentus* water treatment, advanced oxidation processes, photocatalysts, Imidacloprid, persistent organic pollutants

1. Introduction

Pesticides are extensively applied on crops to meet food requirements, yet they are persistent, bio-accumulative, and easily transported over vast distances from their sources, therefore representing a severe risk to environmental habitats but global awareness of this problem is still fragmented.

Imidacloprid (IMI) belongs to the neonicotinoid class of pesticides and is one of the most widely used pesticides. It is applied on various crops, including maize, cotton, rice and other grains, as well as vegetables and fruits to fight insect pests like aphids and thrips. Unfortunately, the widespread usage of Imidacloprid in Pakistan has caused serious environmental pollution. According to the European Food Safety Authority, IMI poses a significant danger to insectivorous and herbivorous birds, as well as granivorous animals and aquatic invertebrates. The impact of IMI on human health is determined by the amount, duration and rate of exposure. IMI can build in enormous quantities in food and drink after being sprayed with high concentrations, causing acute poisoning (e.g., gastrointestinal diseases, neurodegenerative problems,

cardiac arrest, and pulmonary hypertension) and death (Nguyen *et al.,* 2020). IMI has come under fire in past few years for potentially leading to the decline of bees by interfering with their sense of direction, memory, and reproduction mode (Zhang *et al.,* 2022). The European Food Safety Authority (EFSA) has banned the use of imidacloprid in Austria, Denmark, Finland, Belgium, Croatia, Poland, Spain, Romania, Lithuania, and Slovakia due to its noxious effects (EFSA, 2020). The European Commission (the EU's executive branch) banned the use of imidacloprid on pollinator-friendly flowering crops and cereals in May 2013. It went even further in May 2018, banning all outdoor imidacloprid use. In Pakistan, however, IMI is legal and widely utilized to control pests. Thus, efficient methods for eradicating IMI from the environment are urgently needed since it causes a serious risk to human health and the environment (Pang *et al.,* 2020).

Advanced oxidation (AOPs) techniques are being used presently since pollution has significantly increased because self-purification is no longer sufficient for pollution control with simple aerial oxidation. Semiconductor photocatalysis has been acknowledged as one of the green approaches to solving global energy and environmental problems (Cuerda-Correa *et al.,* 2020; Alam and Verma, 2021). Several semiconductor nanomaterials are developing as feasible competing options for such independent and decentralized applications (Tabasum *et al.,* 2021). Because of their appealing characteristics, CuO and ZnO nanoparticles are a potential class of photoactive nanomaterials in the scientific spotlight due to their alluring properties (Alam *et al*., 2017). CuO and ZnO have been recognized as efficient photocatalysts for the degradation of a variety of organic pollutants owing to their unique features, which include having a smaller bandgap, being affordable and non-toxic, possessing photostability, and being easily accessible (Alam *et al*., 2018; Alam *et al*., 2023). CuO has bandgap energy of 2.23 eV whereas bandgap energy of ZnO is 3.6 eV (Okpara and Fayemi, 2019; Amutha *et al*., 2016).

Biological or green methods for the fabrication of nanoparticles offers distinct benefit because they utilize natural resources. Among biological methods, the green preparation of metal oxide NPs by using plant extract has the advantage of being a one-step, simple, affordable, energy-efficient, eco-friendly and more sustainable method. Plant extracts contain phytochemicals such as terpenes, terpenoids, alkaloids, ascorbic acid, reductase, and phenols (David and Moldovan, 2020). These phytochemicals act as capping and stabilizing agents, which play a key role in the green synthesis of CuO and ZnO nanoparticles. The green synthesis of CuO and ZnO nanoparticles can be used for various purposes. For example, *Adiantum lunulatum* was used to prepare CuO for use as a booster for plant defense (Sarkar *et al.*, 2020). *Caesalpinia bonducella* was used to prepare a CuO biosensor for the electrochemical sensing of riboflavin (Sukumar *et al.*, 2020). *Carica papaya* extract was used to fabricate ZnO nanoparticles for electrochemical sensing of silymarin (Sharma *et al.*, 2018). *Myristica fragrans* was used to synthesize ZnO nanoparticles for antiparasitic, antidiabetic, antibacterial, antioxidant and larvicidal properties (Faisal *et al.*, 2021). *Mussaenda frondose* extract to fabricate ZnO NPs is used for cancer and diabetes treatment (Jayappa *et al.*, 2020). *Citrus x paradis* extract to develop ZnO NPs is used to evaluate the electrochemical redox response of SPCE (Okpara *et al.*, 2020).

A. esculentus belongs to family *Malvaceae* of plants and is also commonly known as bhindi, ladyfinger, gumbo, or okra. It is an annual herb and is widely distributed in Africa, America, Asia, and Southern Europe. *Abelmoschus esculentus* leaves are rich in phytochemicals such as phenolic compounds, terpenoids, flavonoids, alkaloids and minerals, which facilitate the biosynthesis of CuO and ZnO nanoparticles. These phytochemicals can donate electrons, facilitating the reduction of metal ions to their zero-valent state. The phytochemicals in the leaves create a stable dispersion of nanoparticles, enhancing their long-term stability and preventing unintended precipitation. *Abelmoschus esculentus* leaves also act as a stabilizing agent because they prevent the agglomeration of nanoparticles by providing a protective coating on the nanoparticle surface, preventing them from clumping together (Maria *et al.,* 2015; Durazzo *et al.,* 2018).

In the present research, we prepared CuO and ZnO nanoparticles using leaf extract of *Abelmoschus esculentus* by hydrothermal method in a simple, single-phase process and their photocatalytic activity for IMI degradation was investigated. To establish optimal conditions for IMI degradation, the photocatalytic degradation of IMI was done under the influence of several parameters such as the effect of pH, photocatalyst dosage and initial concentration of IMI. To the best of our knowledge, there is no report on the utilization of *A. esculentus* leaves extract as a reducing agent in the synthesis of the CuO and ZnO nanoparticles by hydrothermal method and their application in the optimization of photocatalytic degradation of imidacloprid pesticide.

2. Materials and methods

The *A. esculentus* leaves were collected from Jhang, Pakistan. Imidacloprid technical standard (99% purity) was purchased from Sigma-Aldrich. Cu $(NO_3)_2{\cdot}3H_2O$ (≥ 99 %), and Zn $(NO_3)_2{\cdot}6H_2O$ (≥ 99 %) were supplied from Merck Company. All chemicals and reagents were of analytical grade and used without further purification. All the working solutions were prepared with deionized water.

2.1. Preparation of extract

A. esculentus leaves contain phytochemicals such as kaempferol, quercetin, coumarin, chlorogenic acid, caffeic acid and gallic acid. These phytochemicals act as reducing and stabilizing agents, which play a vital role in the green synthesis of copper and nickel nanoparticles (Borokin *et al*., 2022). *A. esculentus* leaves were thoroughly rinsed with deionized water and air-dried for 12 days. The dried leaves were then ground into powder by a mechanical grinder and stored in an airtight jar at room temperature.

The extract was prepared by mixing 5 g of fresh *A. esculentus* leaves powder in 100 mL of distilled water and then heated for 1 hour at 40 °C while being constantly stirred. The resulting solution was concentrated in a rotary evaporator and then filtered three times with Whatman filter sheets. The collected extract was then stored at 4 °C for use in the synthesis of CuO and ZnO nanoparticles in the future.

2.2. Green synthesis of CuO and ZnO nanoparticles by hydrothermal method

The hydrothermal method was used to synthesize CuO and ZnO nanoparticles. For the preparation of CuO nanoparticles, 10 mL of *A. esculentus* extract was mixed with 90 mL of Cu $(NO_3)_2{\cdot}3H_2O$ (0.05 mM) under vigorous stirring and then, added 0.1 M NaOH solution dropwise until the pH value reached 12. Similarly, for the fabrication of ZnO nanoparticles, the same proportion of solutions were taken with Zn $(NO_3)_2{\cdot}3H_2O$ (0.05 mM) in place of Cu $(NO_3)_2{\cdot}3H_2O$ (0.05 mM). The resulting homogenous solutions were transferred into 150 mL capacity autoclave with a Teflon-liner at a temperature of 125 °C for 4 h. After the reaction, the resulting solutions were centrifuged at 5000 rpm for 20 minutes. The pallets containing CuO and ZnO nanoparticles were properly cleaned with de-ionized water three times. The pellets were then heated in an oven at 100 ˚C for 4 h. CuO and ZnO nanoparticles were calcined in a muffle furnace for an hour at 600 C and 550 ˚C, respectively, for efficient crystallization (Abo Zeid *et al.,* 2020). The calcined CuO and ZnO nanoparticles were stored in airtight containers until they were used.

2.3. Characterization method and instrument

The prepared CuO and ZnO nanoparticles were characterized chemically, physically, and morphologically using different analytical techniques such as HR-SEM, FTIR, XRD, TGA, and DTA. The morphologies of prepared nanoparticles were studied by HR-SEM (Stereoscan LEO 440). Fourier Transform Infrared spectrometer (Bruker ALPHA) was used for the identification of functional groups responsible for the reduction of nanoparticles. Thermogravimetric-differential thermal analysis (TG-DTA) was carried out using STA 1500 Rheometric Scientific (England).

2.4. Photocatalytic degradation experiments

Photocatalytic degradation of IMI as a pollutant was carried out employing green synthesized CuO and ZnO nanoparticles using UV light irradiation. 1000 mg L^{-1} stock solution of IMI was prepared in ultrapure water, which was kept at 4 °C without light. The stock solution was diluted with distilled water to make working standards. A closed wooden boxing reactor comprising 8 x18 W UV lamps (ZamZam micro technologies ZM 44W, λ_{max} = 254 nm) was used to perform the photocatalytic degradation experiments. A UV radiometer was used to determine the strength of UV rays (Analytic Jena UVX digital radiometer with UVX-25 probe for 254 nm light). The distance between the UV light source lamp and the test solution was fixed at 10 cm above the solution reactor to maintain a constant light intensity.

For optimum degradation of IMI, various parameters were optimized. The amount of photocatalyst (0.1-0.5 g L^{-1}) was added to the IMI solution in various concentrations (10–70 mg L^{-1}) at a certain pH (5–11) and the irradiation time was 50 min. 150 mL of solution was used in the experiments. For 30 minutes, the suspension was magnetically agitated in the dark to reach an adsorption/desorption equilibrium between the photocatalyst and IMI solution. Aliquots of 5 mL were removed at specific intervals for 50 minutes and then centrifuged at 5000 rpm for 15 minutes to eliminate all photocatalysts from IMI solution. UV-vis measurements using a UV-4000 UV-Vis spectrophotometer was carried out to assess the concentration of IMI at 270 nm (Atwan *et al*., 2019). All experiments were performed in triplicate and had great reproducibility, with just an average error of less than 5%. The percentage degradation was calculated by using the following equation (1):

$$Degradation(\%) = \frac{C_0 - C}{C_0} x\,100 \quad (1)$$

where C_0 and C are the initial and final concentrations of IMI, respectively

The total organic carbon (TOC) of the TMX degraded samples was analyzed by a TOC analyzer (Analytic Gena/Multi N/C 3100). The samples were first treated with HCl to make them acidic, and then they were put into a TOC analyzer (Derbalah *et al*., 2019).

3. Results and discussion

In this study, we used an environmentally friendly approach for the synthesis of CuO and ZnO photocatalysts from *A. esculentus* leaves extract and their photocatalytic activity for the degradation of IMI was investigated to benefit the field of water treatment.

3.1. UV-vis analysis

Figure 1 (a) and (b) illustrates UV-Vis spectra and gap band CuO and ZnO nanoparticles using *A. esculentus* extract. The sharp absorption peaks of synthesized CuO and ZnO nanoparticles at are positioned at 516 and 412 nm respectively. The sharpness of peaks suggested that nanoparticles are stable while higher intensity of peak suggests that yield of both nanoparticles is high. The optical band gap is estimated using Tauc's Equation (2)

$$(\alpha h\nu)^n = A(h\nu - E_g) \quad (2)$$

Where α is absorption coefficient, A is constant, E*g* represents band gap, hν is photon energy and exponent n depends on the type of transition.

The band gap values of CuO and ZnO nanoparticles has been calculated to be about 2.23 eV and 3.6 eV respectively (Okpara *et al*., 2019; Amutha *et al*., 2016). Thus, the prepared nanoparticles are semiconductors that can be utilized as photocatalysts (Sabouri *et al*., 2018) Figure 2 (a) and (b).

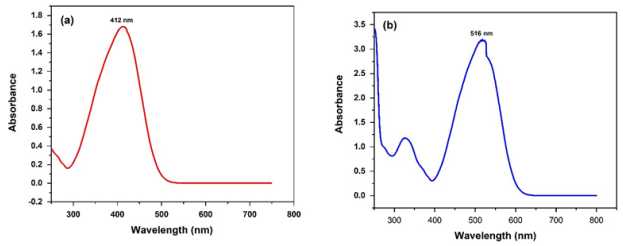

Figure 1. UV-vis spectra of *A. esculentus* leaf-synthesized (a) CuO and (b) ZnO solutions

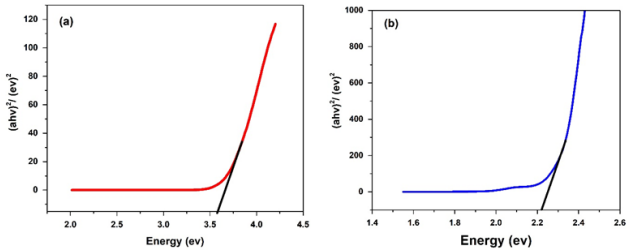

Figure 2. Band gap of *A. esculentus* leaf-synthesized (a) CuO and (b) ZnO solutions

3.2. HR-SEM

HR-SEM was used to examine the surface morphology of produced CuO and ZnO nanoparticles. HR-SEM depicted identical morphology of CuO nanoparticles with spherical shapes while ZnO nanoparticles showed agglomeration as shown in Figure 3 (a) and (b). Similar results were observed from the SEM images of CuO and ZnO nanoparticles produced by native cyclodextrins and *salvia macrosiphon* Boiss extract respectively (Sabouri *et al.,* 2019; Suárez-Cerda *et al.,* 2017). The size distribution of the prepared nanoparticles was evaluated using ImageJ 1.45s software, and the data were displayed as histograms. Figure 4 (a) and (b) showed the average size of CuO and ZnO nanoparticles were in the range of 24–33 nm and 18–35 nm respectively.

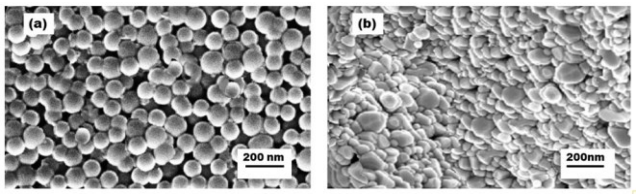

Figure 3. HR-SEM images of *A. esculentus* leaf-synthesized (a) CuO and (b) ZnO nanoparticles

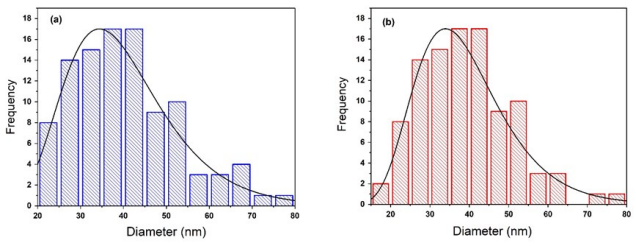

Figure 4. Particle size distribution histogram of *A. esculentus* leaf-synthesized (a) CuO and (b) ZnO nanoparticles

3.3. FTIR analysis

Figure 5 shows the FTIR spectra of CuO and ZnO nanoparticles produced with *A. esculentus* leaf extract. The CuO and ZnO nanoparticles ranged between 435-3756 cm^{-1} and 456-3650 cm^{-1} respectively. FTIR was a range of nanoparticles. The 435 cm^{-1} absorption band is an indication of a Cu–O vibration that stretches. The peaks observed at 752 cm^{-1} represent the vibrational modes of CuO nanostructures, and the C-O and C-N vibrations of the amide-I protein band can be allocated to 1106 cm^{-1} (Iqbal *et al.,* 2021). The presence of a -COOH group and an N-H stretching vibration in amino acids causes peaks of about 1684 and 2359 cm^{-1}. Figure 5 also displays the FTIR spectra study of ZnO nanoparticles. The Zn–O–Zn vibration is confirmed by the absorption band at 456 cm^{-1}. The existence of amide II and amide I of proteins can be assigned to the peaks detected at 1103 and 1502 cm^{-1}, respectively. The presence of N-H stretching vibration in the amino acid of the protein causes the peaks about 2350 cm^{-1}. The low absorption peaks at 3756 and 3650 cm^{-1} could be created by water molecules forming active hydrogen bonds when they adsorb on CuO and ZnO nanoparticles. The FTIR spectra revealed that proteins' amide bands around 1100 cm^{-1} are responsible for the reduction and stability of nanoparticles (Bharathi *et al.,* 2020). Similar results were previously reported from the FTIR spectra of CuO and ZnO nanoparticles produced by *Escherichia sp.* and *Aegle marmelos* leaf extract respectively (Dhayalan *et al.,* 2021; Noman *et al.,* 2020). The presence of organic matter, such as proteins' amide bands around 1100 cm^{-1}, can introduce impurities into the nanoparticle structure. Calcination was carried out to eliminate this organic layer which can improve the stability and reactivity of the nanoparticles.

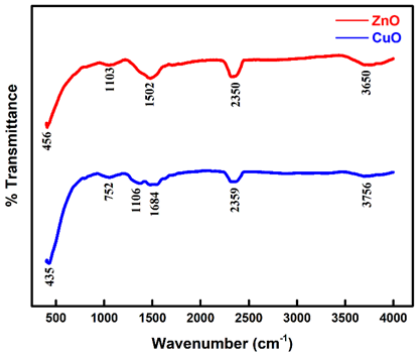

Figure 5. FTIR spectra of *A. esculentus* leaf-synthesized (a) CuO and (b) ZnO nanoparticles

3.4. XRD analysis

The XRD patterns of CuO and ZnO nanoparticles using *A. esculentus* extract are presented in Figure 6. The crystalline planes (100), (102), (110), (103), (200), and (112) are connected with the strong and sharp diffraction peaks of CuO nanoparticles at 2θ =33.45, 49.61, 58.09, 68.56, and 68.11 degrees. At 2θ =36.63 and 39.69 degrees, two high-intensity peaks were observed. The Miller indices (102) and (101), respectively, confirmed that the CuO nanoparticles were monoclinic. Copper nanoparticles indexed to JCPDS card No. 01-080-1268 were also proven to be crystalline, monoclinic, and feature a pure face-centered cubic phase structure (Sorbiun et al., 2018). The (111), (100), (111), (111), (220), (200), (220), and (311) crystalline planes are connected with the intense peaks of ZnO nanoparticles at 2θ =30.2, 34.6, 35.35, 38.2, 52.76, 59.55, and 77.65 degrees. A high-

intensity peak was found at 2θ= 45.45 degrees, with miller indices of 220, indicating that the resultant ZnO nanoparticles have a face-centered cubical structure. The XRD pattern compliance with JCPDS card No. 75- 1526, also confirmed that ZnO nanoparticles are monoclinic and crystalline and have a pure face-centered cubic phase structure (Patel & Patel, 2018). CuO and ZnO nanoparticles had an average particle size of 24.43nm and 28.03nm, respectively, which were determined using the Debye-Scherrer equation (3).

$$D = \frac{0.9 / \lambda}{\beta \cos\theta} \quad (3)$$

where D is crystallite size, λ is the X-ray wavelength (0.1546 nm), β is the full-width at half maximum of the peak in radians (FWHM) and θ is the Bragg diffraction angle.

These results are consistent with previous reports of green synthesis of CuO and ZnO nanoparticles using other plant extracts. (Iqbal *et al.,* 2021; Patel & Patel, 2018; Sorbiun *et al.,* 2018).

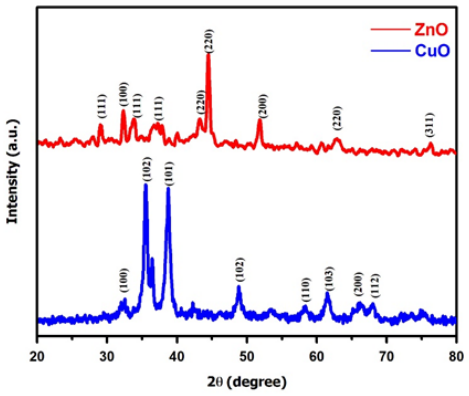

Figure 6. XRD patterns of *A. esculentus* leaf-synthesized (a) CuO and (b) ZnO nanoparticles

3.5. TGA-DTA analysis

TGA-DTA analysis was carried out to find out the thermal stability of phytochemically synthesized NPs when heated at a rate of 15 °C /min in the air at temperatures ranging from 50 to 600 °C. The TGA-DTA curve of CuO nanoparticles is shown in Figure 7 (a). Between 30 and 70 °C, almost 12% of the sample's weight was lost due to moisture removal, while between 250 and 400 °C, nearly 35% of the sample's weight was lost due to the burning of organic matter (*Abelmoschus esculentus* extract). Around 50 °C, there is a tiny endothermic DTA peak, which is the result of the first mass loss in the TGA curve. A strong DTA endothermic peak of about 350 °C is coupled with the second major mass loss in TGA, which occurs between 250 and 400 °C. The TGA-DTA curve of ZnO nanoparticles is shown in Figure 7 (b). Between 30 and 90 °C, about 18 wt% weight loss was noticed due to moisture removal, and almost 35 wt% weight loss was noticed at 300–350 °C due to the burning of the sample's organic matter. Around 90 °C, there is a tiny endothermic DTA peak, which corresponds to the first mass loss in the TGA curve. A strong DTA exothermic peak of about 250–300 °C is connected with the second major mass loss in TGA, which occurs around 300–350 °C (Iqbal *et al*., 2021).

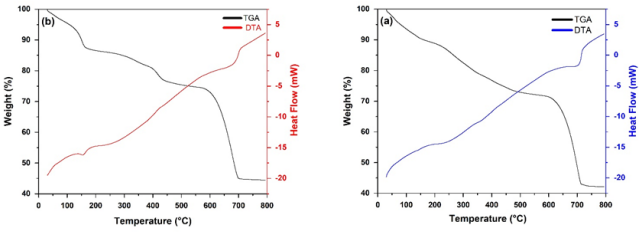

Figure 7. TGA-DTA of *A. esculentus* leaf-synthesized (a) CuO and (b) ZnO nanoparticles

3.6. Optimization of operational parameters

3.6.1. Degradation of IMI under different light conditions

To assess the photocatalytic response of nanoparticles, IMI was removed under pH 9, with different operating conditions such as under dark conditions or UV irradiation, as shown in Figure 8. Experiments exposing IMI solutions to UV irradiation in the absence of a catalyst showed no appreciable decrease in the IMI concentration (<10%) within 50 min of irradiation. Experiments carried out in the dark, but in the presence of 0.3 g semiconductor nanoparticles showed a significant reduction of IMI of 18% for CuO and 10% for ZnO after 50 min. Semiconductor irradiation demonstrated synergistic effects, resulting in a nearly complete reduction of IMI by CuO in only 50 min. In contrast, ZnO had a lower removal capability, achieving only 81 % IMI degradation in 50 min. Metal oxide nanoparticles such as ZnO and CuO nanoparticles are known for their photocatalytic properties. They become more effective at breaking down pesticides in the presence of light, especially ultraviolet (UV) light. Under dark conditions, the absence of light means that the nanoparticles cannot fully harness their photocatalytic potential. They also have restricted contact time. This results in a marginal reduction in their pesticide degradation capabilities compared to when they are exposed to light (Naseem and Durran, 2021).

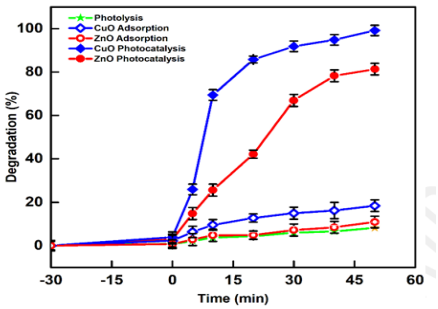

Figure 8. Degradation of 30 mgL^{-1} IMI at pH = 9 using 0.3 gL^{-1} of photocatalyst (◆,◇) CuO, (●○) ZnO. Photocatalysis (filled symbols) or in the dark (empty symbols). Additionally, a blank experiment was also carried out to analyze the effect of effect of (★) direct photolysis

3.6.2. Effect of pH on the photocatalytic degradation of IMI

The effect of pH on the degradation of IMI using CuO and ZnO nanoparticles was studied by changing the pH from 5 to 11 while keeping photocatalyst dosage (0.3 g L^{-1}) and IMI concentration (30 mg L^{-1}) constant. 0.1 M HCl and 0.1 M NaOH solutions were used to keep the pH of various

solutions stable. Figure 9 depicts the degrading efficiency of IMI when the initial pH is varied. The degrading efficiency of IMI was increased from 79.33 to 98.914% by increasing the pH from 5 to 9 and then dropping to 89.7% at pH 11. The efficiency of IMI was increased by using ZnO photocatalyst from 40.08 to 73.87% by changing the pH from 5 to 9, followed by a decrease to 64.86% with pH 11. The results of the present research revealed that pH has a significant impact on the photocatalytic degradation of IMI, which is in line with the findings of Derbalah *et al*. (Derbalah *et al.,* 2019). The pH affects the speciation of target contaminants and the surface charge of catalysts. Furthermore, when the imidacloprid degradation rate was plotted against the pH of the water solution, it was observed that as the pH increased, the photodegradation rate increased. Both catalysts (CuO and ZnO) were found to have the highest degradation efficiency at pH 9. This could have happened because increasing the pH of the hydroxyl ion increased the rate of $^{\bullet}OH$ generation via photo-oxidation through holes in the CuO and ZnO valence bands. These holes interact with the surface bond H_2O to produce $^{\bullet}OH$. Furthermore, in the photocatalytic process, the $^{\bullet}OH$ is expected to be the major oxidizing species.

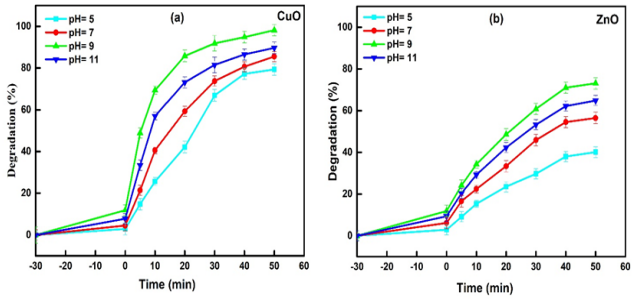

Figure 9. Effect of pH on the degradation of IMI using *A. esculentus* leaf-synthesized (a) CuO and (b) ZnO photocatalyst

3.6.3. Effect of photocatalyst dosage

Understanding the influence of catalyst dose on IMI degradation is critical to reducing capital expenses associated with material use A change in photocatalyst doses at a constant concentration of IMI (30 mg L^{-1}) and pH 9 was used to study the effect of an increase in the photocatalysts dosage on photodegradation of IMI (Figure 10). The efficiency of IMI was increased, from 89.66 percent to 99.73 percent by increasing the catalyst dosage from 0.1 to 0.5 g L^{-1}, by the use of CuO photocatalyst. Whereas, by employing ZnO photocatalyst from 0.1 to 0.5 g L^{-1}, the degradation of IMI was increased from 62.67 to 81.43 %. The results showed that the rate of imidacloprid photocatalytic degradation increased with increasing CuO and ZnO photocatalyst dosage. At lower catalyst charges, IMI degradation is minimal as more light is transmitted and less transmitted radiation is utilized to degrade the photocatalyst. The faster degradation rate is due to the availability of more active sites with higher catalyst concentrations and the increased number of IMI molecules adsorbed. Increased generation of electrons, holes and hydroxyl radicals causes IMI to degrade faster. These findings are in agreement with those reported by Wang *et al*. (Wang *et al.,* 2020).

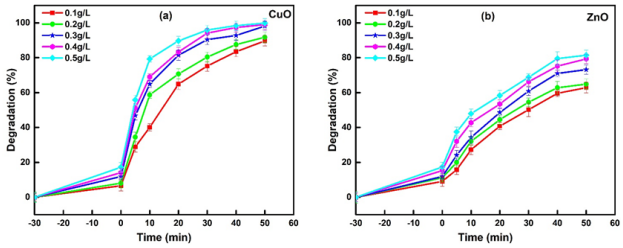

Figure 10. Effect of photocatalyst dosage on the degradation of IMI using *A. esculentus* leaf-synthesized (a) CuO and (b) ZnO photocatalyst (Photocatalyst dosage = 0.1–0.5 g L^{-1}, IMI = 30 mg L^{-1}, pH = 9)

3.6.4. Effect of initial concentration of IMI

The degradation of IMI using CuO and ZnO photocatalysts was studied by increasing the initial concentration of IMI (10-70 mg L^{-1}) while pH (9) and photocatalyst dosage (0.3 g L^{-1}) remained constant. Figure 11 depicts the results of both catalysts at various initial IMI concentrations. The photocatalytic degradation of IMI using CuO and ZnO photocatalyst was reduced from 99.59 to 80.01% and 79 to 62% after 60 min respectively with increasing the IMI concentration from 10 to 70 mg L^{-1}. The effect of the concentration of IMI on the photocatalytic degradation of IMI was carried out by changing the initial concentration of IMI (10-70 mg L^{-1}) at constant pH (9) and photocatalyst dosage (0.3 g L^{-1}). When the concentration of the target pollutant (IMI) is increased, degradation efficiency decreases because a larger number of molecules react with the same number of oxidants created by the same number of catalytic sites. Furthermore, the presence of organic substances that absorb radiation can obstruct photon transit while also lowering the rate of oxidant production (Derbalah *et al.,* 2019). Despite the drop in removal percentage achieved after photocatalytic treatment, the suggested photocatalysts may effectively degrade IMI across a wide range of ambient concentrations. The performance of CuO and ZnO nanoparticles are compared with literature work and it is presented in Table 1.

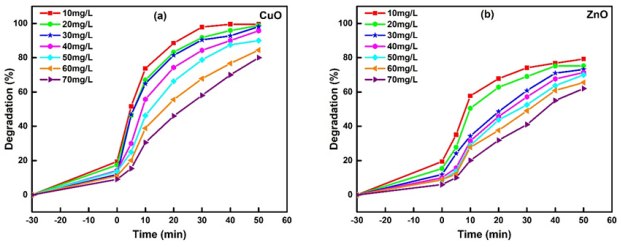

Figure 11. Effect of concentration of IMI on the degradation of *A. esculentus* leaf-synthesized (a) CuO and (b) ZnO photocatalyst (Photocatalyst dosage = 0.3 g L^{-1}, IMI = 10–70 mg L^{-1}, pH = 9)

The degradation mechanism of imidacloprid (IMI) by CuO and ZnO nanoparticles typically involves a series of chemical reactions and surface interactions between the nanoparticles and the pesticide molecule. IMI molecules initially adsorb onto the surface of nanoparticles. This adsorption is facilitated by the presence of active sites on

the nanoparticle surface, such as hydroxyl groups or other functional groups. Once adsorbed, IMI molecules undergo activation through interactions with metal oxide sites. This activation involves the breaking of specific chemical bonds within IMI. CuO and ZnO nanoparticles act as redox catalysts, facilitating electron transfer reactions. IMI undergoes oxidation or reduction reactions on the nanoparticle surface. These reactions result in the formation of intermediate products. The degradation process generates intermediate products that are different from the parent IMI molecule. These intermediates have lower toxicity and are eventually degraded or mineralized. The final complete mineralization of IMI takes place, converting it into non-toxic end products like water and carbon dioxide (Liu *et al.,* 2021).

Table 1. Comparison of present work with the literature

Systems	pH	Catalyst dosage	$[IMI]_0$ (mg L^{-1})	Lamp	Time Removal (min)	Degradation %	Reference
UV/TiO_2	5	200 mg L^{-1}	20	15W, λmax = 254 nm	180	90.24	(Shorgoli & Shokri, 2017)
UV/ZnO	11	50 mg L^{-1}	5.5	UV light at 365 nm.	60	47	(Atwan *et al.,* 2019)
Dielectric barrier discharge/ Cu^{+2}	6.7	50 mg L^{-1}	50	75V	480	75.6	(Li, 2018)
ZnO(nano)/ H_2O_2/artificial sunlight	7	1000 mg L^{-1}	1	300 W Xenon lamp	480	97	(Derbalah *et al.,* 2019)
ZnO(normal)/H_2O_2/artificial sunlight	7	1000 mg L^{-1}	1	300 W Xenon lamp	480	72	(Derbalah *et al.,* 2019)
UV-activated persulfate (UV/PS)	6.42	0.25mM	2.5	Hg lamp with 75 W λmax = 253.7 nm)	20	90	(Wang *et al.,* 2020)
UV-activated peroxymonosulfate (UV/PMS)	6.42	0.25mM	2.5	Hg lamp with 75 W λmax = 253.7 nm)	20	66.7	(Wang *et al.,* 2020)
UV/CuO	11	300 mg L^{-1}	30	44W, λ_{max} = 254 nm	50	99	Present study
UV/ZnO	11	300 mg L^{-1}	30	44W, λ_{max} = 254 nm	50	80	Present study

3.6.5. TOC analysis

Total organic carbon (TOC) analysis was carried out to examine the mineralization of photo-degraded IMI solution using CuO and ZnO nanoparticles at optimum conditions (Photocatalyst dosage = 0.5g, pH = 9, IMI conc. 30mgL^{-1} and contact time = 50 min). The mineralization of IMI was calculated to be 92 and 76% by using CuO and ZnO nanoparticles respectively as shown in Figure 12 (a). Mineralization of IMI showed pseudo first-order kinetic model as shown in Figure 12 (b). The TOC reduction indicates the efficiency of CuO and ZnO nanoparticles for the mineralization of IMI solution.

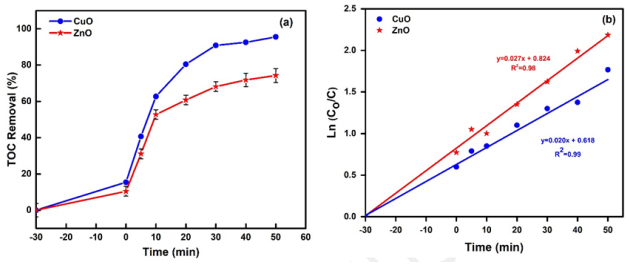

Figure 12 (a) TOC removal efficiency (%) of IMI *A. esculentus* leaf-synthesized CuO and ZnO nanoparticles at optimum conditions (Photocatalyst dosage = 0.5g, pH = 9, IMI Conc. 30mgL^{-1} and contact time = 50 min). **(b)** plot of ln (C_o/C) versus t (time) of IMI using CuO and ZnO nanoparticles.

3.7 Reusability and photostability of CuO and ZnO photocatalysts

The photostability and reusability of any photocatalyst are essential features for their commercial applications. Figure 13 shows the synthesized CuO and ZnO nanoparticles showed high photostability and reusability during five photocatalytic cycles using fresh solutions containing IMI. After the degradation of IMI, the photocatalysts were centrifuged and then washed thrice with ultra-pure water. The regenerated photocatalysts were then dried in a vacuum oven at 100°C for three hours. The regenerated photocatalysts retained their photocatalytic degradation ability even after 5 consecutive cycles, revealing that these photocatalysts are inexpensive and eco-friendly. A little decrease in the effectiveness of the reused catalyst might be owing to the deposition of hydroxides on the photocatalyst active sites, which can block and impede its active sites.

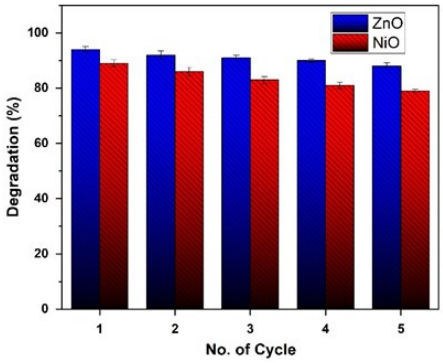

Figure 13. Reusability of *A. esculentus* leaf-synthesized CuO and ZnO photocatalysts up to five cycles against IMI

4. Conclusion

A simple, economical, and eco-friendly method is adopted to synthesize stable CuO and ZnO nanoparticles using *A.*

esculentus leaf extract by hydrothermal method. Their effectiveness was assessed from the degradation of IMI pesticides. The UV-Vis absorption peak was identified at 516 and 412 nm. HR-SEM showed identical morphology of CuO nanoparticles with spherical shapes while ZnO nanoparticles showed agglomeration. The average size of CuO and ZnO nanoparticles calculated were in the range of 24–33 nm and 18–35 nm respectively which was confirmed by HR-SEM and XRD. FTIR analysis showed the involvement of phytochemicals such as kaempferol, quercetin, coumarin, chlorogenic acid, caffeic acid and gallic acid in the preparation and stability of nanoparticles. Furthermore, the green synthesized CuO and ZnO nanoparticles showed a fascinating photocatalytic degradation of IMI. The findings showed that CuO (99%) had stronger photocatalytic activity than ZnO (81%) but ZnO had higher long-term stability. A comparison of the photocatalytic degradation of CuO and ZnO photocatalysts revealed that the degradation of IMI using a CuO photocatalyst is faster than using a ZnO photocatalyst but both catalysts are promising, economical, and sustainable options for water treatment.

Conflict of Interest

All authors declare no conflict of interest.

Acknowledgement

The authors are thankful to HEC and Government College University, Faisalabad, Pakistan.

Data Availability Statement

The data that support the findings of this study are available from the corresponding author upon reasonable request.

References

Abo Zeid E.F., Nassar A.M., Hussein M.A., Alam, M.M., Asiri A.M., Hegazy, H.H. and Rahman M.M. (2020). Mixed oxides CuO-NiO fabricated for selective detection of 2-aminophenol by electrochemical approach, *Journal of Materials Research and Technology*, **9**, 1457–1467.

Alam U. and Verma N. (2021). Direct Z-scheme-based novel cobalt nickel tungstate/graphitic carbon nitride composite: Enhanced photocatalytic degradation of organic pollutants and oxidation of benzyl alcohol, *Colloids and Surfaces A: Physicochemical and Engineering Aspects*, **630**, 127606.

Alam U., Khan A., Ali D., Bahnemann D., and Muneer M. (2018). Comparative photocatalytic activity of sol-gel derived rare earth metal (La, Nd, Sm and Dy)-doped ZnO photocatalysts for degradation of dyes, *RSC Advances*, **31**, 17582–17594.

Alam U., Khan A., Raza W., Khan A., Bahnemann D. and Muneer M. (2017). Highly efficient Y and V co-doped ZnO photocatalyst with enhanced dye sensitized visible light photocatalytic activity, *Catalysis Today*, **284**, 169–178.

Alam U. Pandey A. and Verma N. (2023). An anthraquinone-integrated S-scheme-based $NiTiO_3$-g-C_3N_4 composite with enhanced hydrogen production activity, *International Journal of Hydrogen Energy*, **48**, 2532–2541.

Amutha C., Thanikaikarasan S., Ramadas V., Bahadur S.A., Natarajan B. and Kalyani R. (2016). Synthesis, characterization and antibacterial efficiency of ZnO nanoparticles using rice as soft bio-template, *Optik*, **10**, 4281–4286.

Atwan A.A., Elmehasseb I.M., Talha N.I. and El-kemary M. (2019). Parameters affecting the photodegradation rate of imidacloprid catalyzed by ZnO nanoparticles, *Journal of Materials and Environmental Sciences*, **10**, 485–494.

Bharathi D., Preethi S., Abarna K., Nithyasri M., Kishore P. and Deepika K. (2020). Bio-inspired synthesis of flower shaped iron oxide nanoparticles (FeONPs) using phytochemicals of *Solanum lycopersicum* leaf extract for biomedical applications, *Biocatalysis and Agricultural Biotechnology*, ***27***, 101698.

Borokini F.B., Oladipo G.O., Komolafe O.Y., Ajongbolo K.F. and Oladipo M.C. (2022). *Abelmoschus esculentus* Moench L. leaf inhibited lipid peroxidation and deproteination, and caused dose-dependent spermatogenesis and impaired hormonal synchronism in Wistar rats, *Applied Food Research*, **2**, 100179.

Cuerda-Correa E.M., Alexandre-Franco M.F. and Fernández-González C. (2020). Advanced oxidation processes for the removal of antibiotics from water, An overview. *Water (Switzerland)*, **12**.

David L. and Moldovan B. (2020). Green synthesis of biogenic silver nanoparticles for efficient catalytic removal of harmful organic dyes, *Nanomaterials*, **10**, 202.

Derbalah A., Sunday M., Chidya R., Jadoon W. and Sakugawa H. (2019). Kinetics of photocatalytic removal of imidacloprid from water by advanced oxidation processes with respect to nanotechnology, *Journal of Water and Health*, **17**, 254–265.

Dhayalan M., Selvaraj M., Karthick K.B., Mohammed R.S.U. and Sillanpää M. (2021). Eco friendly synthesis and characterization of zinc oxide nanoparticles from *Aegle marmelos* and its cytotoxicity effects on MCF-7 cell lines, *Nanofabrication*, **6**, 44–51.

Durazzo A., Lucarini M., Novellino E., Souto EB., Daliu P. and Santini A. (2018). Beneficial Properties — Focused on Antidiabetic Role — For Sustainable Health Applications, *Molecules*., **24**, 38.

EFSA. (2020). Pesticides: EFSA to examine emergency use of neonicotinoids.

Faisal S., Jan H., Shah S.A., Shah S., Khan A., Akbar M.T., Rizwan M., Jan F., Wajidullah N., Khattak A. and Syed S. (2021). Green Synthesis of Zinc Oxide (ZnO) Nanoparticles Using Aqueous Fruit Extracts of *Myristica fragrans*: Their Characterizations and Biological and Environmental Applications, *ACS Omega*, **6**, 9709–9722.

Iqbal A., Haq A., Antonio G., Ali S., Naqvi R. Westerhoff P. and Garcia-segura S. (2021). Green Synthesis of Flower-Shaped Copper Oxide and Nickel Oxide Nanoparticles via *Capparis decidua* Leaf Extract for Synergic Adsorption-Photocatalytic Degradation of Pesticides, *Catalysts*, **11**, 806.

Jayappa M.D., Ramaiah C.K., Kumar M.A.P., Suresh D., Prabhu A., Devasya R.P. and Sheikh S. (2020). Green synthesis of zinc oxide nanoparticles from the leaf, stem and in vitro grown callus of Mussaenda frondosa L.: characterization and their applications, *Applied Nanoscience (Switzerland)*, **10**, 3057–3074.

Li K. (2018). Degradation of imidacloprid in wastewater by dielectric barrier discharge system, *IOP Conference Series: Earth and Environmental Science*, **128**.

Liu S., Yu W., Cai H., Lai F., Fang H. and Huang H. (2021). A comparison study of applying natural iron minerals and zero-valent metals as Fenton-like catalysts for the removal of

imidacloprid, *Environmental Science and Pollution Research*, **28**, 1–13.

Nguyen D.D.D., Huynh K.A., Nguyen X.H. and Nguyen T.P. (2020). Imidacloprid degradation by electro-Fenton process using composite Fe_3O_4–Mn_3O_4 nanoparticle catalyst, *Research on Chemical Intermediates*, **46**, 4823–4840.

Maria E.E.C., Luciana M.P., de S., Elba S.F., Amanda P.F., Carlos A.A.G. and Jailane S.A. (2015). Nutritional, antinutritional and phytochemical status of okra leaves (*Abelmoschus esculentus*) subjected to different processes, *African Journal of Biotechnology*, **8**, 683–687.

Naseem T. and Durrani T. (2021). Environmental Chemistry and Ecotoxicology The role of some important metal oxide nanoparticles for wastewater and antibacterial applications : A review, *Environmental Chemistry and Ecotoxicology*, **3**, 59–75.

Noman M., Shahid M., Ahmed T., Niazi M.B.K., Hussain S., Song F. and Manzoor I. (2020). Use of biogenic copper nanoparticles synthesized from a native *Escherichia sp*. as photocatalysts for azo dye degradation and treatment of textile effluents, *Environmental Pollution*, **257**, 113514.

Okpara E.C. and Fayemi O.E. (2019). Comparative study of spectroscopic and cyclic voltammetry properties of CuONPs from citrus peel extracts, *Materials Research Express*, **6**, 105056.

Okpara E.C., Fayemi O.E., Sherif E.S.M., Junaedi H. and Ebenso E.E. (2020). Green wastes mediated zinc oxide nanoparticles: Synthesis, characterization and electrochemical studies. *Materials*, **13**.

Pang S., Lin Z., Zhang Y., Zhang W., Alansary N., Mishra S., Bhatt P. and Chen S. (2020). Insights into the toxicity and degradation mechanisms of imidacloprid via physicochemical and microbial approaches, *Toxics*, **8**, 1–31.

Patel N.A. and Patel I.B. (2018). X-Ray Studies of Zinc Oxide (ZnO) Nanoparticles grown by Hydrothermal Technique. *International Journal of Research Culture Society*, **2**, 87–90.

Sabouri Z., Akbari A., Hosseini H. and Darroudi M. (2018). Facile green synthesis of NiO nanoparticles and investigation of dye degradation and cytotoxicity effects, *Journal of Molecular Structure*, **1173**.

Sabouri Z., Fereydouni N., Akbari A., Hosseini H. A., Hashemzadeh A., Amiri M.S., Oskuee R.K. and Darroudi M. (2019). Plant-based synthesis of NiO nanoparticles using *Salvia macrosiphon* boiss extract and examination of their water treatment, *Rare Metals*, **39**, 1134–1144.

Sarkar J., Chakraborty N., Chatterjee A., Bhattacharjee A., Dasgupta D. and Acharya K. (2020). Green synthesized copper oxide nanoparticles ameliorate defence and antioxidant enzymes in *lens culinaris, Nanomaterials*, **10**, 312.

Sharma D., Sabela M.I., Kanchi S., Bisetty K., Skelton A.A. and Honarparvar B. (2018). Green synthesis, characterization and electrochemical sensing of silymarin by ZnO nanoparticles: Experimental and DFT studies, *Journal of Electroanalytical Chemistry*, **808**, 160–172.

Shorgoli A.A. and Shokri M. (2017). Photocatalytic degradation of imidacloprid pesticide in aqueous solution by TiO_2 nanoparticles immobilized on the glass plate, *Chemical Engineering Communications*, **204**, 1061–1069.

Sorbiun M., Shayegan Mehr E., Ramazani A. and Taghavi S. (2018). Green synthesis of zinc oxide and copper oxide nanoparticles using aqueous extract of oak fruit hull (jaft) and comparing their photocatalytic degradation of basic violet 3, *International Journal of Environmental Research*, **12**, 29–37.

Suárez-Cerda J., Espinoza-Gómez H., Alonso-Núñez G., Rivero I. A., Gochi-Ponce Y., Flores-López L. Z., Espinoza-go H., Alonso-nu G., Sua J., Suárez-Cerda J., Espinoza-Gómez H., Alonso-Núñez G., Rivero I. A., Gochi-Ponce Y. and Flores-López L. Z. (2017). A green synthesis of copper nanoparticles using native cyclodextrins as stabilizing agents, *Journal of Saudi Chemical Society*, **21**, 341–348.

Sukumar S., Rudrasenan A. and Nambiar D.P. (2020). Green-synthesized rice-shaped copper oxide nanoparticles using *Caesalpinia bonducella* seed extract and their applications, *ACS Omega*, **5**, 1040–1051.

Tabasum A., Alghuthaymi M., Qazi U.Y., Shahid I., Abbas Q., Javaid R., Nadeem N. and Zahid M. (2021). Uv-accelerated photocatalytic degradation of pesticide over magnetite and cobalt ferrite decorated graphene oxide composite, *Plants*, **10**, 6.

Wang Q., Rao P., Li G., Dong L., Zhang X., Shao Y., Gao N., Chu W., Xu B., An N. and Deng J. (2020). Degradation of imidacloprid by UV-activated persulfate and peroxymonosulfate processes: Kinetics, impact of key factors and degradation pathway, *Ecotoxicology and Environmental Safety*, **187**, 109779.

Zhang Y., Zeng D., Li L., Hong X., Li-Byarlay H. and Luo S. (2022). Assessing the toxicological interaction effects of imidacloprid, thiamethoxam, and chlorpyrifos on *Bombus terrestris* based on the combination index, *Scientific Reports*, **12**, 1–9.